and copper appear on a rather large scale with tending to be assemblies.

In terms of correlation with geology and each element, the anomalous values of gold are distributed outer and/or inner limits of diorite-granodiorite body, and of silver in the Oyotun Volcanics and intrusive rocks. It should be noted that in the Pena Verde zone gold and silver anomalies are distributed with a relatively high concentration in the silicified zones adjoining to the diorites. The majority of lead anomaly is found out in the Oyotun Volcanics and instrusive rocks with a single anomalous point in the Mesozonic sedimentary rocks. Overall, the distribution of lead anomalous zones are widely dispersed, except to the east of Pena Verde where relatively high concentration was observed. Zinc and molybdenum are distributed throughout the area, with the tendency to gather around fissures and intrusive rocks. Geochemical anomaly of copper nearly corresponded to the alteration zones in the Oyotun Volcanics. In Pena Verde, the copper anomaly corresponds to the above-mentioned silver anomalous zone, and to the monzonite intrusion area in La Huaca, and is relatively gathered within the basement and its peripheral intrusive rocks in Paramo.

From the viewpoint of zonal arrengements of geochemical anomaly, around La Huaca the copper anomalous zones are surrounded by those of zinc, which in turn are sorrounded by those of lead. In Pena Verde, the tendency is that the silver anomaly is surrounded by the copper anomaly.

2-2 Geophysical Survey

2-2-1 Purpose of the Survey

The purpose of the CSAMT survey is to elucidate resistivity structure and to explore porphyry copper deposit.

2-2-2 Method of the Survey

1) Scope of the survey

The geophysical survey area is shown in Fig. Ⅱ-7.

The scope of the survey is as follows:

Area:	21km²
Station interval:	300m to 1000m
Number of station:	71 points

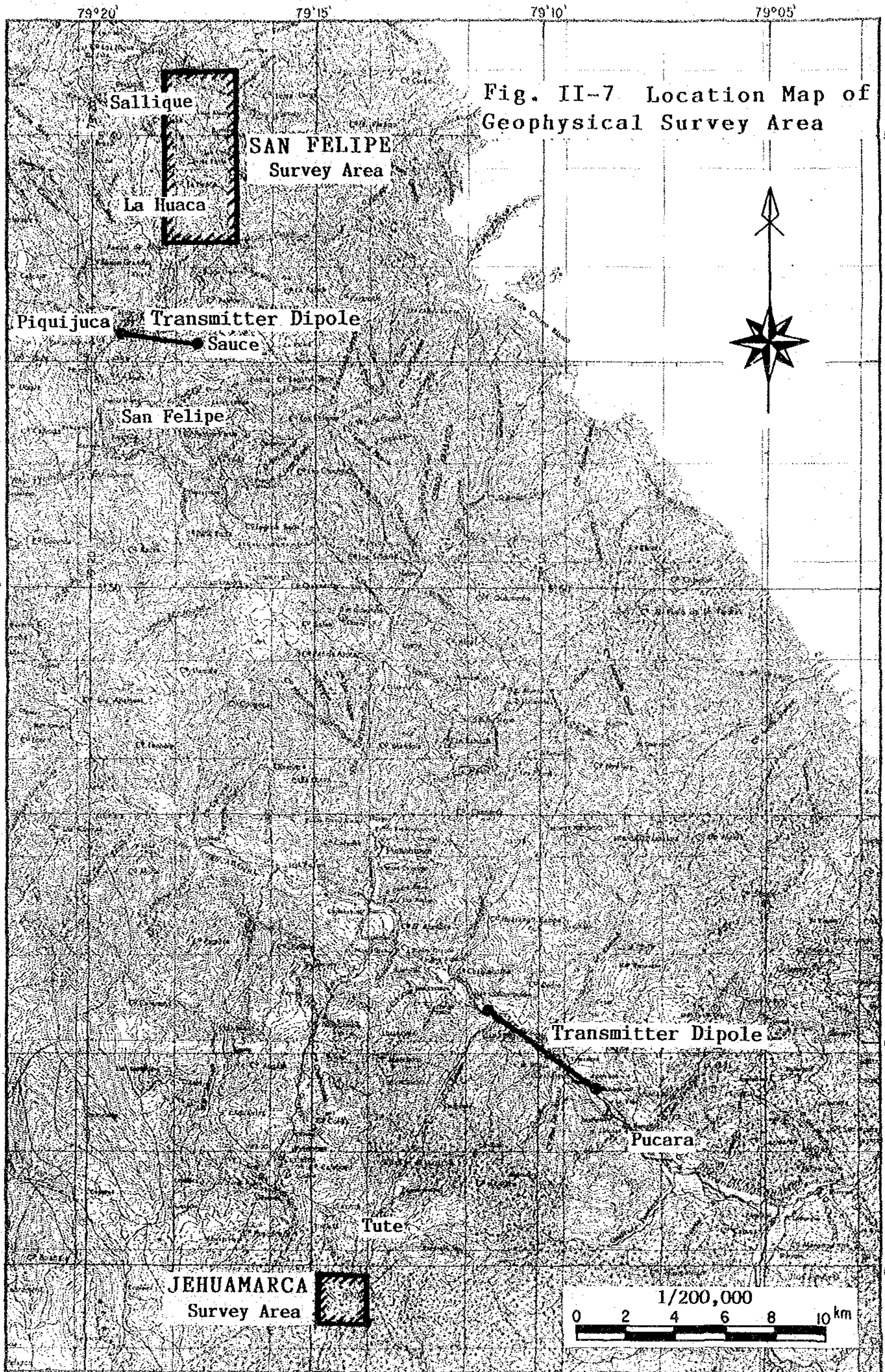

Fig. II-7 Location Map of Geophysical Survey Area

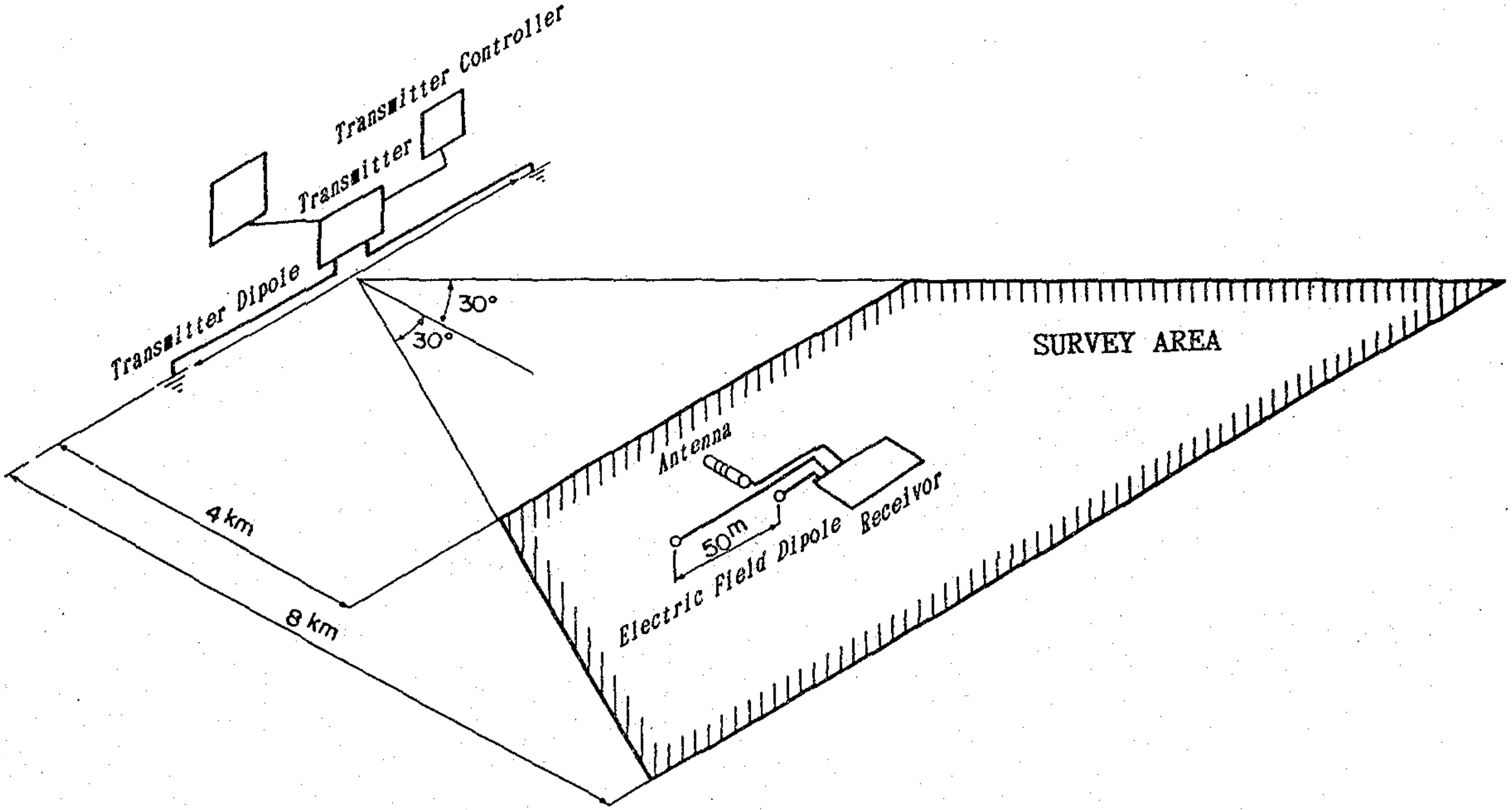

Fig.II—8 Schematic Diagram of CSAMT Survey

Survey stations are densely distributed around La Huaca and Pena Verde of the survey area and sparsely distributed in the center of the survey area (see Fig. II-10).

2) Method of CSAMT survey

Controlled Source Audio Frequency Magnetotelluric method (called CSAMT) is a kind of magnetotelluric method with a controlled electromagnetic source. One horizontal electric field and one magnetic field, which are orthogonal to each other, are measured in ten different frequencies and apparent resistivity of each frequency is calculated.

General configuration of CSAMT survey is illustrated in Fig. II-8.

Goldstein and Strangway (1975) described CSAMT method in detail.

The specifications of CSAMT survey are as follows:

(a) Signal source

Electrode: 3,200m long, N105° E direction

Electrode Material: At each Electrode, 10 holes (about 1.5m deep) were dug. Zinc plates (1.5m×2.0m) were buried with mixture of water, salt and bentonite in each hole.

Resistance of entire transmitting bipole system: 16 ohms

Transmitting current: Transmitting electric current of each frequency is as follows:

Frequency(Hz)	4	8	16	32	64	128	256	512	1024	2048
Bipole(Ampere)	12	12	12	12	12	12	12	10	10	5

(b) Signal reception

Reception mode: TE mode (electrical dipole direction is parallel general strike of geological structure).

Distance from a source bipole: Distance between a survey station and the source is over 4 km.

Potential dipole: Electrode separation is 50 m and is parallel to then direction of a transmitting bipole.

Magnetic sensor: Ferrite core coil.

Frequency: 4, 8, 16, 32, 64, 128, 256, 512, 1024, 2048 Hz

Recording time: Over 20 minutes.

Repetition of measurements: Measurements were repeated at least three times for each frequency at a station.

3) Equipment

Equipments used for the survey are manufactured by Zonge Engineering & Research Organization.

They are as follows:

(a) Transmitter

Engine generator (ZMG-7.5)

output power 30 kVA, 120/400 Hz, 3 phases, 53 HP (at 3,600 rpm)

Transmitter (GGT-6)

maximum output 5 kw, 24 A, 1,000 V

Transmitter controller (XMT-2)

frequency range: DC to 10,000 Hz

(b) Receiver

Data processor (GDP-12)

amplifier, filter

Magnetic sensor

core coil, sensitivity 0.2 mV/gamma Hz

2-2-3 Data Reduction and Analysis

Data reduction and analysis were carried out as the flow chart (see Fig. Ⅱ-9).

The symbols used for this report are as follows:

ρ : true formation resistivity (Ωm)

ρa : apparent resistivity (Ωm)

$\rho a'$: apparent resistivity after near field correction (Ωm)

f : frequency (Hz)

Ex : electric field (μV/m)

Hy : magnetic field (nT)

d : skin depth (m)

r : distance between a transmitter bipole and a receiving station (m)

K(r) : geometric constant

h_1 : thickness of the first layer (m)
ρ_1 : resistivity of the first layer (Ωm)
ρ_2 : resistivity of the second layer (Ωm)
ω : angular frequency ($2\pi f$)
μ : magnetic permeability ($4\pi \times 10^{-7}$ H/m)

1) Calculation and average of apparent resistivity

Apparent resistivity, ρa, is calculated as follows:

$$\rho a = \frac{1}{5f}\left(\frac{Ex}{Hy}\right)^2 \quad \text{------------ ①}$$

Measurements were repeated for each frequency at a station and an apparent resistivity at a station of respective frequency was decided by geometrically averaging over three well-repeated field data. Apparent resistivity values are listed in Table. II-3.

2) Near field correction

Resistivity value, thus obtained, include near field effect and do not show true magnetotelluric apparent resistivity in lower frequencies, if distance between a receiving station and a transmitting bipole is near, less than three-fold of a skin depth.

$$d = 503\sqrt{\frac{\rho}{f}} \quad \text{---------------- ②}$$

Influence of near field effect is large in resistive area. Near field effect is seen in the data of the all station in the San Felipe Zone. Near Field effect is corrected by the following equation, ③, by assuming homogeneous and isotropic earth.

$$\rho a' = K(r) \cdot r \cdot \left(\frac{Ex}{Hy}\right)^2 \quad \text{---------- ③}$$

3) EM analysis

The mean field correction, stated above, can reduce only over-shoot of mean field effect and cannot reduce under-shoot of apparent resistivities at those frequencies a little higher than three-fold of a skin depth frequency. The under-shoot part of apparent resistivity curves is interpreted by a direct electromagnetic interpretation method of Anderson's algorism (1982).

4) Inversion

Apparent Resistivity vs. frequency curves of the all stations are inverted one-dimensionally into horizontally layered earth.

One-dimensionally inversion was automatically performed as follows:

An apparent resistivity vs. frequency curve of an initial horizontally layered earth model is calculated by a computer. Then the calculated curve is compared with a field data. Usually the two has some difference. A computer looks for a more suitable horizontally layered earth model. And repeat calculation until two apparent resistivity curves match each other. Thus obtained most fitted horizontally layered earth model is one of the answers to a given field data.

The forward equation for a two-layer earth model is as follows:

$$\rho_s = \rho_1 \cdot \cot h^2 \ (c_1 h_1 + \cot h^{-1} c_1 / c_2)$$

where,

$$c_1 = \sqrt{\frac{J \omega \mu}{\rho_1}}$$

$$c_2 = \sqrt{\frac{J \omega \mu}{\rho_2}}$$

The results of One-dimensional inversion of the all stations are tabulated in Apx. 11 at the end of this report.

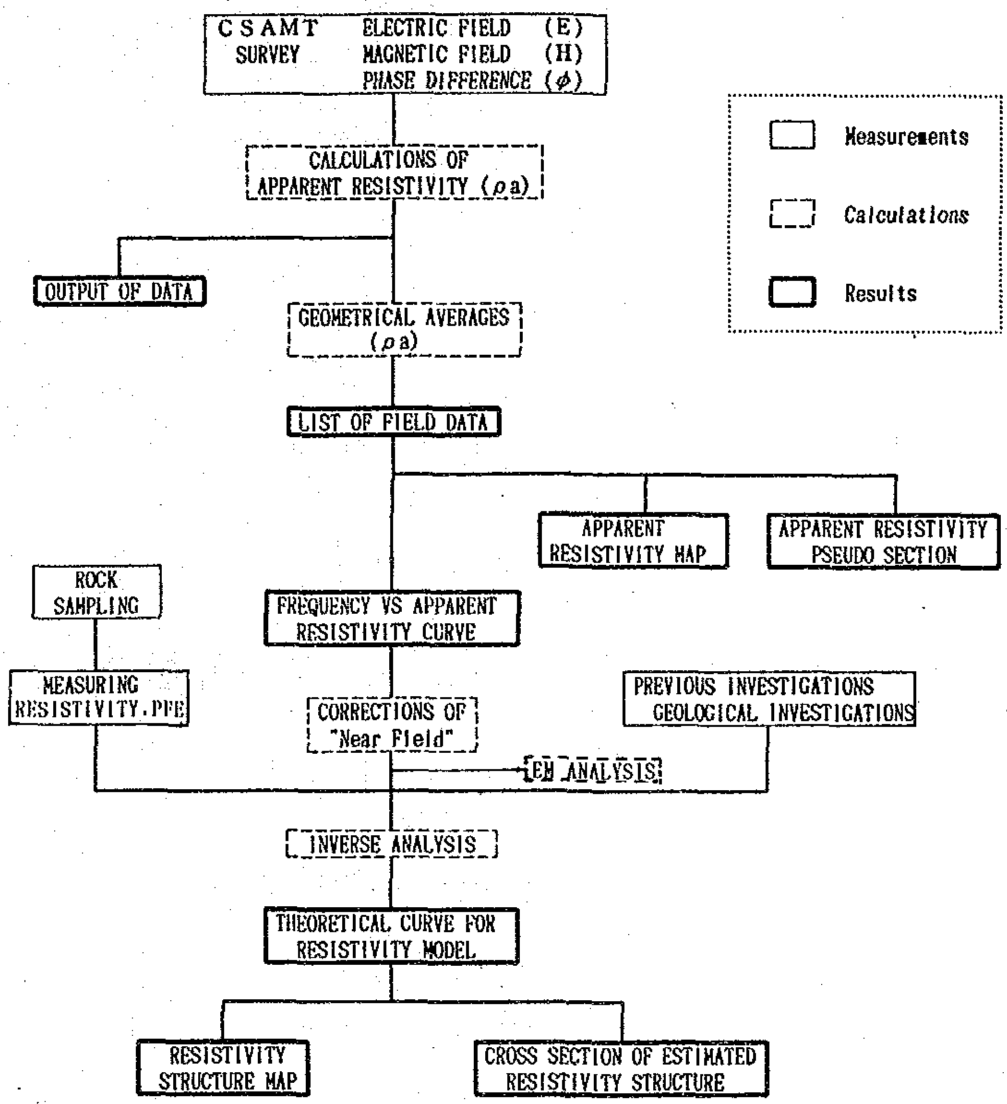

Fig.II−9 Flow Chart for CSAMT Data Processing

Table.II－3 List of Apparent Resistivity

ST.NO. & DIPOLE	FREQUENCIES (HZ)									
	4	8	16	32	64	128	256	512	1024	2048
1 S	1444	760	458	331	259	193	149	111	88	78
2 S	23670	13250	8723	6924	6075	4595	3917	3663	3635	3525
3 S	5929	3426	2341	1920	1656	1245	852	654	399	347
4 S	3181	3323	3502	3363	3065	2267	1902	1929	2379	2973
5 S	9149	4771	2911	2171	1859	1364	1050	773	547	427
6 S	9449	5752	4235	3537	3056	2314	1932	1636	1300	976
7 S	2164	1117	660	435	309	196	126	84	65	54
8 S	810	415	238	169	140	109	94	95	103	111
9 S	660	366	230	173	148	124	119	123	123	123
10 S	1329	729	469	371	340	307	302	319	320	335
11 S	736	437	307	247	220	184	161	122	88	73
12 S	631	343	223	179	167	160	173	208	235	265
13 S	442	301	241	209	188	162	167	206	248	258
14 S	2120	1139	704	543	493	465	460	410	428	343
15 S	1994	1180	794	625	548	479	448	403	382	448
16 S	504	307	222	177	149	121	108	92	84	88
17 S	456	242	144	114	103	93	93	89	76	80
18 S	592	302	171	124	111	101	105	117	123	157
19 S	2432	1245	708	508	477	471	474	425	377	327
20 S	7564	4808	3313	2448	1997	1728	1703	1569	1337	1034
21 S	3913	1570	833	610	634	627	828	1095	1184	941
22 S	852	565	450	415	420	441	489	479	389	266
23 S	1869	925	447	286	274	291	305	296	264	223
24 S	1557	747	367	215	203	204	210	189	158	139
25 S	1642	791	393	246	220	226	263	266	218	146
26 S	772	383	222	145	145	162	180	220	228	209
27 S	202	96	68	59	62	74	87	104	108	119
28 S	1009	536	317	242	239	239	246	250	263	271
29 S	808	464	324	252	236	208	195	175	155	170
30 S	217	161	134	112	99	87	195	116	164	250
31 S	6592	3619	2229	1569	1209	808	539	355	239	171
32 S	4365	2341	1402	947	725	488	319	205	134	94
33 S	3928	2140	1276	861	640	411	273	190	138	108
34 S	6425	3469	2265	1940	1616	1169	904	801	775	718
35 S	234	125	77	57	48	40	43	51	58	65
36 S	61	32	19	15	17	22	34	44	47	42
37 S	14	5.8	2.7	3.1	6.9	11	17	24	33	43
38 S	309	145	63	40	52	59	63	65	64	68
39 S	293	151	73	41	55	57	51	46	40	73
40 S	394	181	77	51	80	84	85	79	74	64
41 S	1040	582	335	235	259	256	248	211	198	192
42 S	2392	1156	579	410	495	517	315	505	454	436
43 S	4356	2404	1366	972	931	890	932	878	812	763
44 S	5397	2983	1853	1451	1404	1417	1335	1297	978	778
45 S	2375	1133	481	344	449	510	568	495	441	996
46 S	1986	1014	517	410	642	601	598	487	422	288
47 S	45	25	12	11	20	23	20	20	28	4.0
48 S	140	65	27	22	43	45	56	55	63	22
49 S	474	213	75	52	90	79	76	68	68	68
50 S	9236	6473	4386	2889	2704	2473	1910	1439	1012	668
51 S	3.3	1.6	0.66	0.93	2.1	2.7	3.0	4.4	11	2.4
52 S	201	102	46	42	74	83	88	84	80	69

Table.II−3 List of Apparent Resistivity

ST.NO. & DIPOLE	FREQUENCIES (HZ)									
	4	8	16	32	64	128	256	512	1024	2048
53 S	8402	4940	2551	1907	2914	3406	3414	3236	2874	2555
54 S	3494	1928	970	685	1026	1032	1444	1174	1033	906
55 S	518	310	179	134	177	225	215	238	220	167
56 S	2432	538	240	168	262	318	360	396	309	315
57 S	618	255	92	83	151	164	180	160	113	100
58 S	3150	1466	519	376	734	628	672	681	642	528
59 S	411	198	63	45	91	84	188	30	820	4581
60 S	258	113	43	34	57	49	51	53	57	56
61 S	403	196	83	111	134	119	137	133	120	108
62 S	49	24	7.9	7.9	11	8.4	12	12	12	11
63 S	885	282	106	123	198	205	170	144	158	198
64 S	723	294	114	139	227	289	205	214	165	165
65 S	263	187	96	84	112	146	149	181	239	74
66 S	553	247	82	80	144	146	137	160	135	195
67 S	4736	2193	814	624	906	880	937	800	754	490
68 S	569	292	93	61	84	64	66	68	66	53
69 S	591	234	48	39	100	88	109	106	95	89
70 S	540	287	99	68	122	106	110	205	720	1453
71 S	670	498	233	149	182	159	200	143	115	84
72 J	23	28	39	50	62	78	69	103	95	105
73 J	14	22	31	44	56	65	89	106	110	106
74 J	29	49	77	104	145	200	276	247	225	204
75 J	35	37	52	76	117	167	212	373	411	315
76 J	76	79	106	144	190	183	203	192	197	212
77 J	25	32	44	58	66	88	108	105	97	61
78 J	31	40	45	68	85	96	93	85	101	116
79 J	64	86	126	184	252	216	194	187	195	187
80 J	17	26	34	46	54	66	76	95	97	94
81 J	16	24	34	49	59	61	62	69	71	56
82 J	14	23	36	56	59	97	121	108	125	190
83 J	33	43	56	80	88	85	104	95	97	108
84 J	25	34	38	58	67	87	151	174	148	127
85 J	14	20	33	47	60	62	64	60	59	45
86 J	47	77	123	192	243	288	239	247	252	207
87 J	26	43	74	102	136	175	180	186	165	191
88 J	75	110	156	229	242	265	288	273	274	226
89 J	27	44	64	88	110	136	149	126	103	22
90 J	24	34	50	73	100	91	100	124	105	67
91 J	112	133	173	215	266	333	331	212	162	90
92 J	37	57	85	110	142	187	242	242	202	151
93 J	46	60	84	115	153	161	191	175	167	113
94 J	26	28	46	62	70	99	106	135	109	71
95 J	15	24	33	51	74	112	133	144	133	123
96 J	22	39	56	100	125	163	169	162	160	120
97 J	12	17	24	35	47	53	78	76	95	96
98 J	34	52	72	105	153	194	204	171	153	144
99 J	52	75	105	140	186	234	210	178	145	109
100 J	21	28	42	60	80	94	111	98	88	74
101 J	22	28	45	62	102	135	154	146	133	109
102 J	19	31	46	62	77	112	116	82	63	54

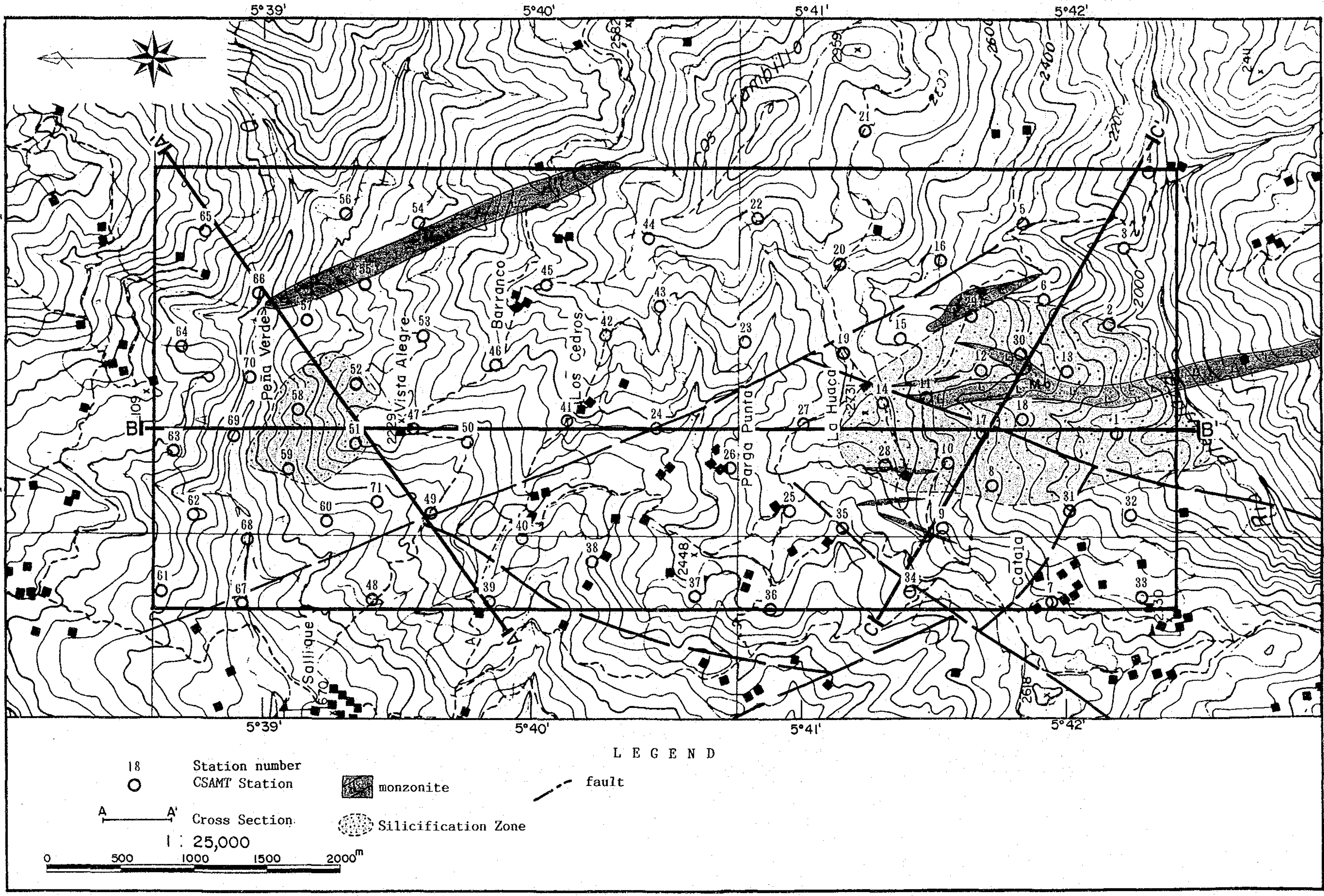

Fig.II--10 Location Map of CSAMT Station in The San Felipe Area

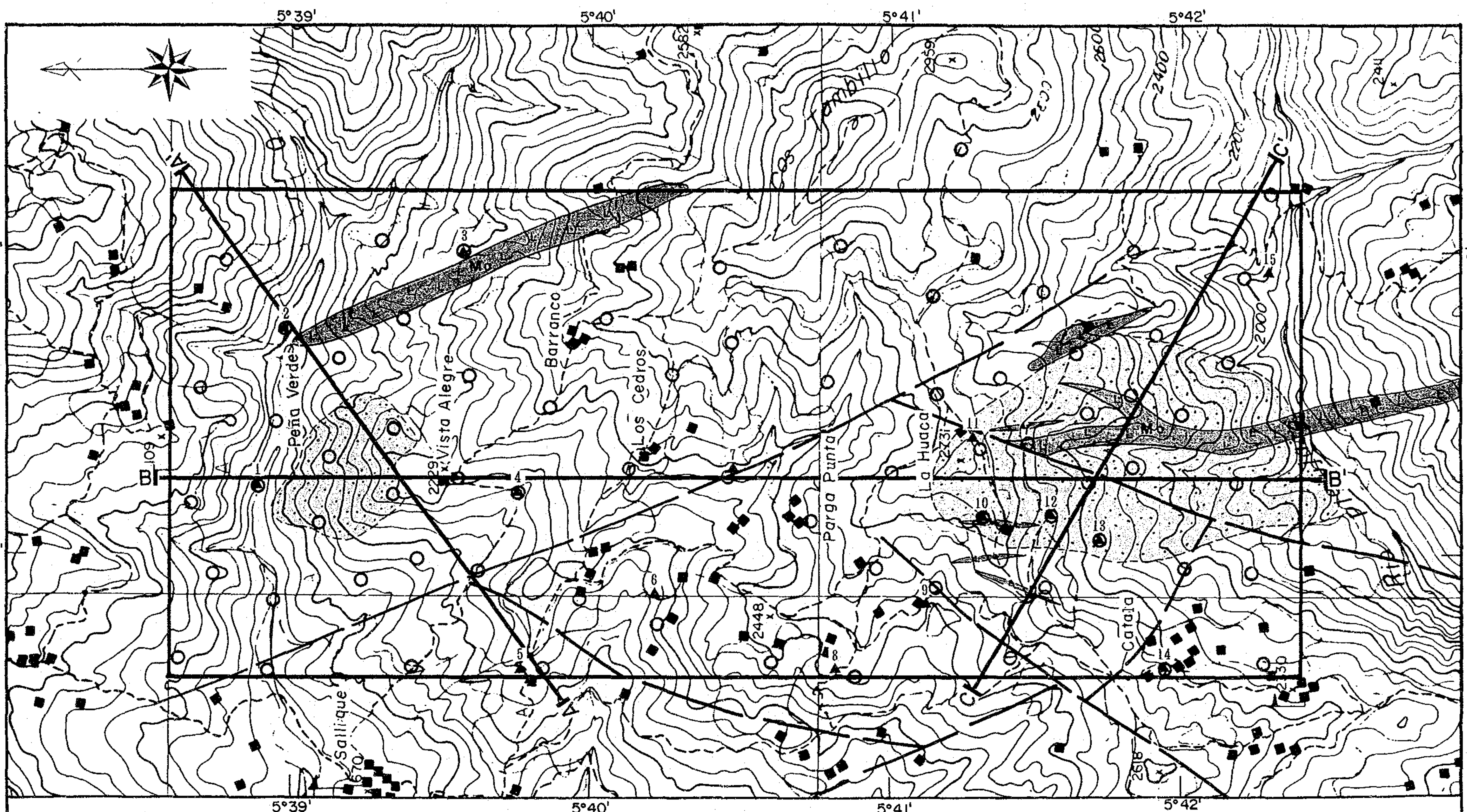

L E G E N D

- CSAMT Station
- A–A' Cross Section
- monzonite
- Silicification Zone
- fault
- 9 Sampling number
- ▲ Sampling Station

1 : 25,000

0 500 1000 1500 2000m

Fig.II−11 Location Map of Rock Sample in The San Felipe Area

Table.II−4　　Result of Rock Properties

No.	Loction	Rock Name	Resistivi-ty(Ω・m)	P F E (%)
1	San Felipe	lapilli tuff	349	2.9
2	San Felipe	monzonite	385	0.6
3	San Felipe	granodiorite	817	2.0
4	San Felipe	silicified andesite	687	1.4
5	San Felipe	sandstone	110	2.5
6	San Felipe	silicified andesite	1,183	2.5
7	San Felipe	silicified rock	8,054	0.5
8	San Felipe	calcareous sandstone	2,049	1.8
9	San Felipe	quartz monzonite	2,655	2.3
10	San Felipe	silicified rock	427	1.7
11	San Felipe	silicified rock	2,478	0.0
12	San Felipe	silicified rock	1,272	0.2
13	San Felipe	silicified andesite	3,711	1.5
14	San Felipe	calcareous sandstone	13,987	1.8
15	San Felipe	granite	1,898	0.8
16	Jehuamarca	lapilli tuff	868	2.3
17	Jehuamarca	tuffaceous silicified rock	2,445	0.3
18	Jehuamarca	lapilli tuff	304	10.8
19	Jehuamarca	argillized lapilli tuff	398	3.3
20	Jehuamarca	argillized lapilli tuff	253	2.5

2-2-4 Results of Survey and Analysis

1) Physical properties of rock samples

Fifteen samples of representative rock-types in the survey area were tested in the laboratory for their resistivity and IP effect. The results are shown in Table II-4 and Fig. II-17.

The rock samples were collected at the points shown in Fig. II-11.

The laboratory measurements are summarized as follows:

Resis-tivity	San Felipe				jehuamarca			
	Rock Name	N	Resis-tivity (Ωm)	FE (%)	Rock Name	N	Resis-tivity (Ωm)	FE (%)
L	monozonite lapilli tuff sndstone	1 1 1	300 300 100	0.6 2.9 2.5	lapilli tuff	4	400	2.3 - 10.8
M	granodiorite		1,000	2.0		1		
H	silified rock silified andesite calcareous sandstone quartz monozonite granite	4 3 2 1 1	3,000 2,000 8,000 3,000 2,000	0 - 1.7 1.4- 2.5 1.8 2.3 0.8	tuffaceous silicified rock		2,000	0.3
Total		15				5		

i) Silicified rock (quartz rock) samples show high resistivity.

ii) Monzonite, tuff and sandstone samples show low resistivity.

iii) Siliceous rock samples show low FE values.

iv) Monzonite, granodiorite and lapilli tuff have 2 to 3 % of FE values. Traces of pyrite can be observed in these rock samples under a magnifier.

2) Apparent resistivity distribution

Apparent resistivity generally at higer frequency reflects the resistivity structure of relatively shallow ground, and of deeper ground at lower frequency.

As the result of measurement, we obtained apparent resistivity distributions at ten frequencies, all of which show a similar tendency over the area generally. Of these the apparent resistivity distributions at three frequencies, 4 Hz, 64 Hz and 1,024 Hz, which most reflect local variation are described in the following section. For the convinience of explanation apparent resistivity values are divided into five groups as below:

10	100	500	5,000	(Ωm)
very low resistivity L L	low resistivity L	medium resistivit M	high resistivity H	very high resistivity H H

Apparent resistivity distribution at 4 Hz (see Fig. II-12 (1))

i) Apparent resistivity values at 4 Hz are a range between 3 and 20,000 Ωm.

ii) General isopleths in N-S direction are shown for this apparent resistivity distribution. In La Huaca and Pena Verde isoplethic curves in NE-SW direction are also observed.

iii) Apparent resistivity higher than 500 Ωm covers most of the survey area except around La Huaca, Pena Verde and at the center and the western area where apparent resistivity is medium and lower.

iv) The medium apparent resistivity zone observed around La Huaca is surrounded by zones of high apparent resistivity, higher than 500 Ωm, and very high apparent resistivity, higher than 5,000 Ωm. It is actually, therefore, a relatively low apparent resistivity zone. This medium apparent resistivity and high apparent resistivity zones surrounding it are arranged in NE-SW direction, where mainly monzonite intrusive veins are at the surface.

v) The trend of apparent resistivity lower than 100 Ωm observed around Pena Verde has also been observed in NW-SE direction in addition to the NE-SW. These low apparent resistivity zones are mainly distributed in small-scale andesite instrusive veins at the surface.

vi) Low apparent resistivity has been observed at only one station in the center and western part of the survey area. Medium apparent resistivity zones that surround it tend to be in N-S direction.

vii) Around the south flange of the survey area as well as in its center and eastern part, some very high apparent resistivity zones, higher than 5,000 Ωm, are distributed.

Apparent Resistivity Distribution at 64 Hz (see Fig. II-12 (2))

i) No apparent resistivity data at 64 Hz is over 5,000 Ωm, thus being lower in average than those at 4 Hz. Three groups of apparent resistivities, medium, high and low, occupy nearly the same distribution areas.

ii) No significant change is observed from the data measured at 4 Hz in the distribution tendency indicated by isoplethic curves.

iii) The medium apparent resistivity distribution observed around La Huaca at 4 Hz extends in broader zones in both NE-SW and N-S directions.

iv) The low apparent resistivity distribution observed around Pena Verde at 4 Hz contains very low apparent resistivity zones, lower than 10 Ωm, extending in N-S direction. Also observed is the tendency for the low apparent resistivity to extend in NE-SW and N-S lines together with medium resistivity distribution over a relatively broad area.

v) The low apparent resistivity observed at 4 Hz in the center and western part of the survey area also contains very low apparent resistivity values less than 10 Ωm. In addition, its distribution area is fairly large, extending north-south (N-S) direction and reaching to the low apparent resistivity zones of Pena Verde.

vi) Around the south flange of the survey area as well as in its center and eastern part high apparent resistivity zones are dominant.

Apparent Resistivity Distribution at 1,024 Hz (see Fig. II-12 (3))

i) Apparent resistivity distribution at 1,024 Hz is similar to that at 64 Hz, but medium apparent resistivity zones are more extensive, very low apparent resistivity zones disappears and low and high apparent resitivity areas are reduced.

ii) Low apparent resistivity zone is surrounded by the medium apparent resistivity zone around La Huaca, which emphasizes its trend in NE-SW direction.

iii) The low apparent resistivity zone in Pena Verde is found between high apparent resistivity zones, emphasizing its trend in NE-SW direction.

iv) Compared with apparent resistivity distributions at 4 Hz and 64 Hz, the low apparent resistivity zones in the center and western parts of the survey area clearly show a trend of distribution in N-S direction.

3) Apparent resistivity pseudo-sections (Fig. II-14)

Three sections, A-A', B-B' and C-C', indicated in each map, were prepared. Each section illustrates the apparent resistivity data in order from the highest to the lowest frequencies, thus representing the variation in apparent resistivity values from the surface down.

The sections give an outline of underground distribution tendency and relative depth with respect to the medium and low apparent resistivity data collected around La Huaca and Pena Verde:

i) In La Huaca, medium apparent resistivity zones are distributed over large area surrounded by those of relatively higher apparent resistivity, and contain relatively lower apparent resistivity scattered in very reduced areas.

ii) In Pena Verde, the low apparent resistivity area is surrounded by relatively higher apparent resistivity, and contains very low apparent resistivity zones in deep. These very low apparent resistivity zones show a slight constriction as they near the ground surface.

4) Analytical results

An under-shoot was observed in the proximity of Pena Verde in the apparent resistivity vs. frequency curve obtained from the measurement results. This under-shoot is generally found in area about a range of several times of the skin depth. It can be identified by a calculation based on EM theory, taking the distance from the transmitting source into consideration.

Fig. II-13 shows an example of calculation based on EM theory using a two-layer structure model (a 80Ωm on top of a 800 Ωm layer) which was created giving a resistivity contrast ten times the value measured at the station 40. Locally descending curvatures can be clearly observed around 16 Hz and 32 Hz. If a direct MT inversion is conducted with this model as is, there will be an erroneous result interpreted as if there were a three-layer structure that would contain a pseudo low resistivity layer against the original two-layer structure. To verify whether the descending curvatures observed in the apparent resistivity vs. frequency curve have been caused by the undershoot or due to a true resistivity structure, a geological interpretation is needed. In this survey we assessed that the observed result was due to the presence of under-shoot development and not caused by underground structure because of the following reasons:

i) curves typical to under-shoot were observed; ii) these curves were found over a broad extent; and iii) if it is analyzed as is, low resistivity layers would have to be assumed to exist throughout different strata of sedimentary rocks, pyroclastic rocks and those intrusive, especially in the granodiorites; this will be a very unnatural result.

Our analysis was conducted based on this assessment.

As a result of the analysis, it is assumed that in the survey area the resistivity section consists of three layers of high, medium and low resistivities.

Sections and plan maps of this resistivity structure consisting of three layers are explained below:

A-A' Section (see Fig. II-14)

This section cuts the low resistivity zones around Pena Verde in NE-SW direction. It is observed that sedimentary rocks, pyroclastic rocks and granodiorite are distributed from the west toward the east through the section.

Medium resistivity layers are assumed to extend broadly from the surface to a great depth except a distribution of silicified and argillized alteration zones around the station 51 and a small-scale low resistivity layer in the shallow part of the surface layers which coincides with the intrusion of andesites. In the south of the station 57 the medium resistivity layer is divided into the surface layer and its lower layer. Under this medium resistivity layer a relatively higher resistivity layer, of around 300 to 800 Ωm, is assumed. This high resistivity layer was not observed near the stations 51 and 52 where pyroclastic rocks are distributed.

B-B' Section (see Fig. II-14)

This section cuts the survey area in N-S direction. Distribution of pyroclastic rocks is found throughout this section. Low resistivity layers are assumed to be both around Pena Verde and La Huaca.

In La Huaca, low resistivity layers of between 50 to 100 Ωm are found between the stations 1 and 10, and around the station 27 near the shallow part of the surface layer at a maximum depth of 500 meters. Below these layers there is a medium resistivity layer of 100 Ωm or higher. The low resistivity layer to the south from around the station 10 corrsponds to the distribution of monzonite and of alteration zones. In the north from the station 10 to the proximity of Pena Verde, a relatively higher resistivity layer, above approximately 700 Ωm, lies as the bottom layer, under the medium resistivity layer.

C-C' Section (see Fig. II-14)

This section is in NW-SE direction to traverse across the low resistivity zones in La Huaca. The section extends across pyroclastic rocks and monzonite, granodiorite and granite which are intruded into the pyroclatic rocks.

The low resistivity layer found near the surface at the station 17 is deeper at the stations 18 and 30. This low resistivity layer is located at the center of the argillized alteration zones, corresponding to the place where monzonites intruded. The medium resistivity layer, of several hundreds Ωm, found around the above conductive layer is in depth around the station 30 to the station 9 and lies between two relatively higher resistivity layers of 800 Ωm or more. These high resistivity layers correspond to the distributions of granite and diorite on the eastern part of the section.

Resistivity Structure Map

For general representation of the resistivity results interpreted at each station, resistivity structure maps have been prepared at the levels of elevation of 2,000 and 1,500 meters.

In addition, distribution maps of low resistivity layers have been drawn to clearly define those found around La Huaca and Pena Verde since part of them may not appear in the structure maps above.

The general view of the resistivity structure maps are as follows:

Resistivity Structure Map (Elevations of 2,000 and 1,500 meters) (see Fig. II-15)

i) As it is obvious from B-B' and C-C' sections, low Resistivity layer was found around La Huaca near the surface. While it shows a trend in NE-SW and N-S directions in the resistivity structure map at a level of 2,000 meters, at a level of 1,500 meters it can be seen to run in NE-SW and NW-SE directions.

ii) Around Pena Verde, the low resistivity layer, of 20 Ωm or less, found at near the surface is distributed around Vista Alegre on a smaller scale.

iii) The low resistivity layers, of 100 Ωm or less, in the center and west extend in NS direction with a relatively extensive distribution covering the elevation from 2,000 to 1,500 meters, and further extend from NE to SW encompassing the low resistivity layers around Pena Verde.

Low Resistivity Distribution Map (see Fig. II-16)

i) The area of low resistivity layers found at La Huaca coincides with the distribution of monzonite located in the center of argillized alteration zones, and other low resistivity layers are distributed in their surrounding proximity.

ii) The distribution of low resistivity layers, of 20 Ωm or less, found at Pena Verde corresponds to the small-scale intrusive body of andesites and lies in a narrow band between silicification zones developed around them.

iii) Low resistivity layers, of 100 Ωm or less, are extensively found in the center and western parts of the area, and are connected to the low resistivity layers at Pena Verde mentioned earlier. These low resistivity layers coincide with the section existing between the pyroclastic and sedimentary rocks in their location and direction.

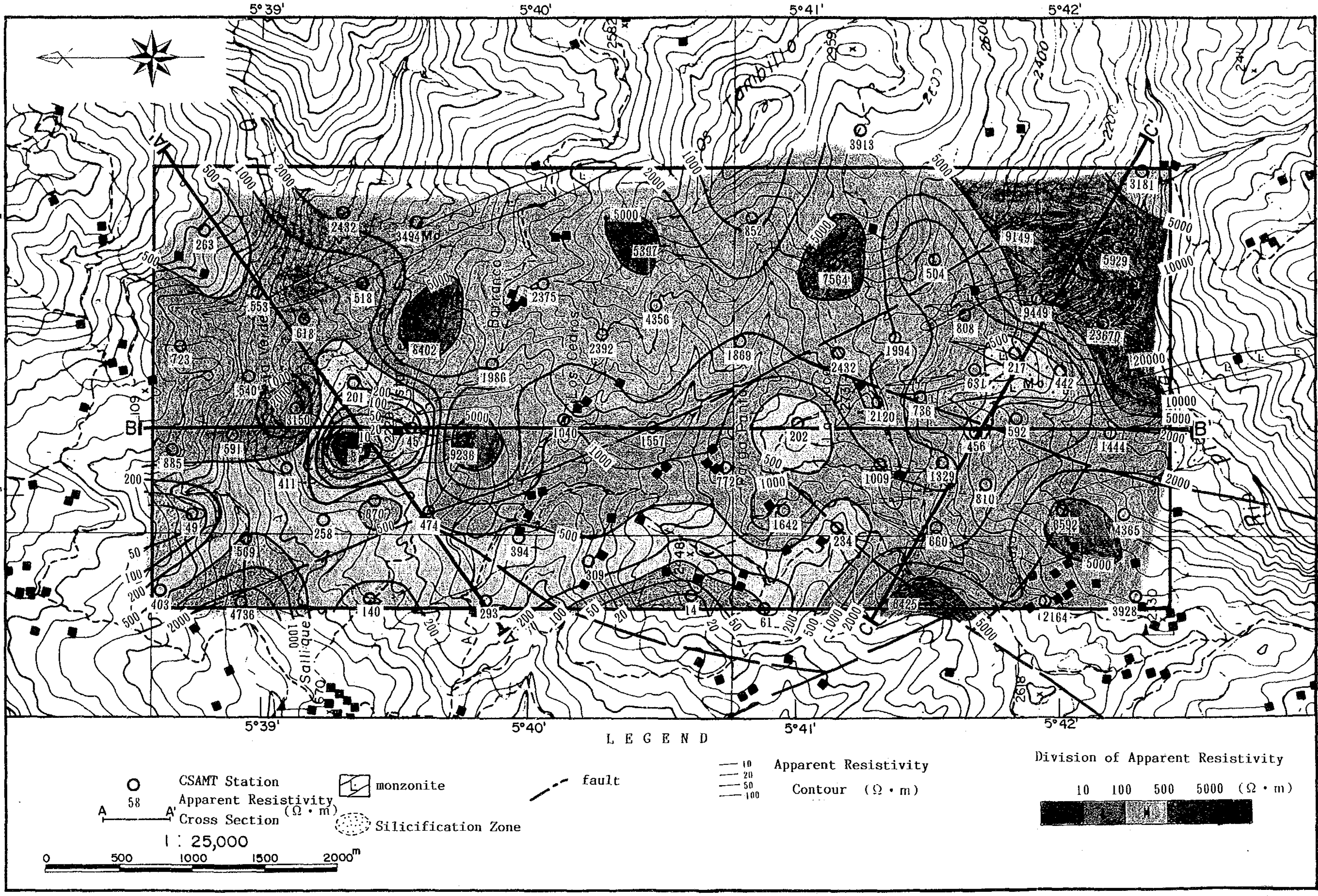

Fig.II−12 (1) Apparent Resistivity Map of The San Felipe Area (Frequency 4Hz)

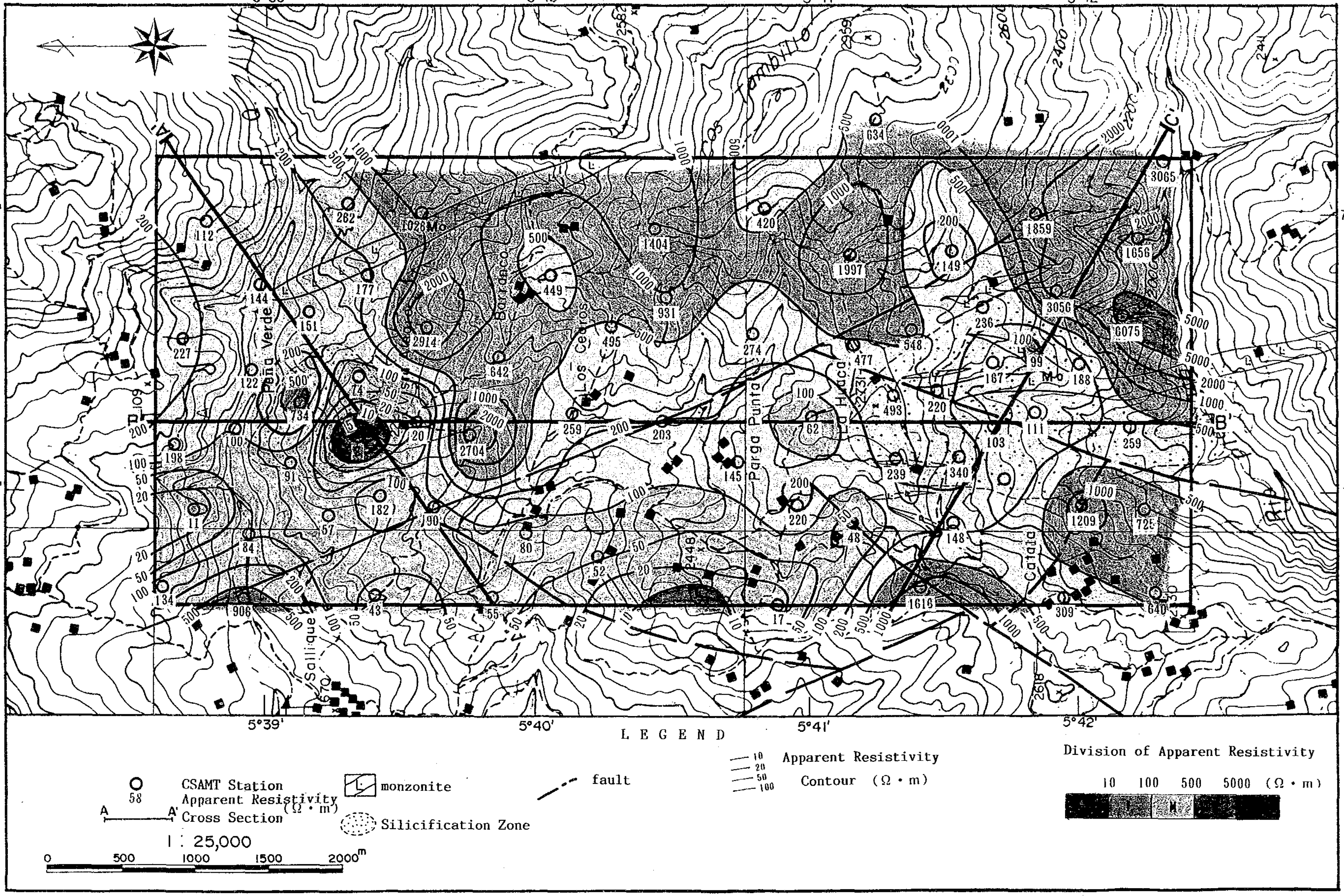

Fig.II-12 (2) Apparent Resistivity Map of The San Felipe Area (Frequency 64Hz)

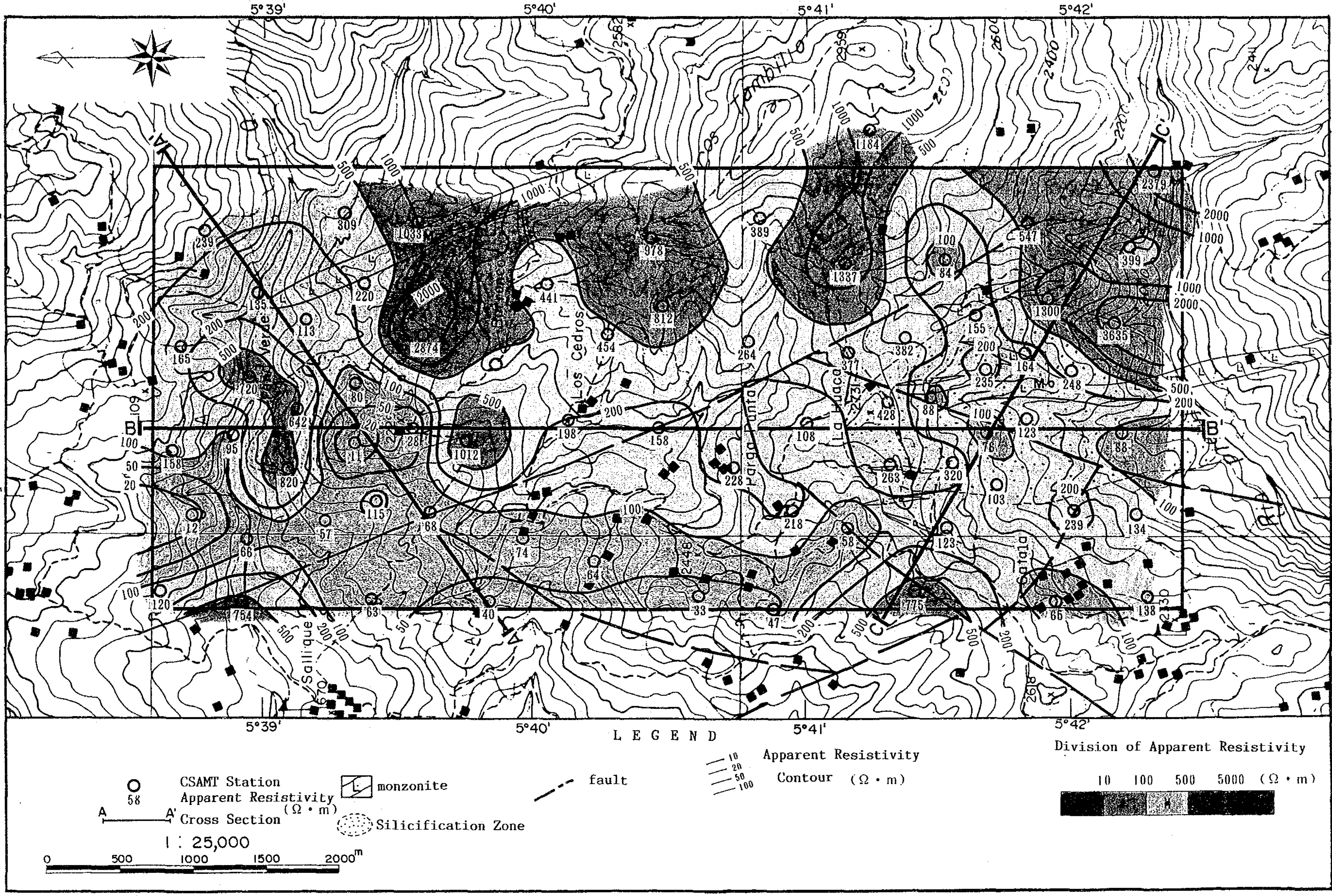

Fig.II−12 (3) Apparent Resistivity Map of The San Felipe Area (Frequency 1024Hz)

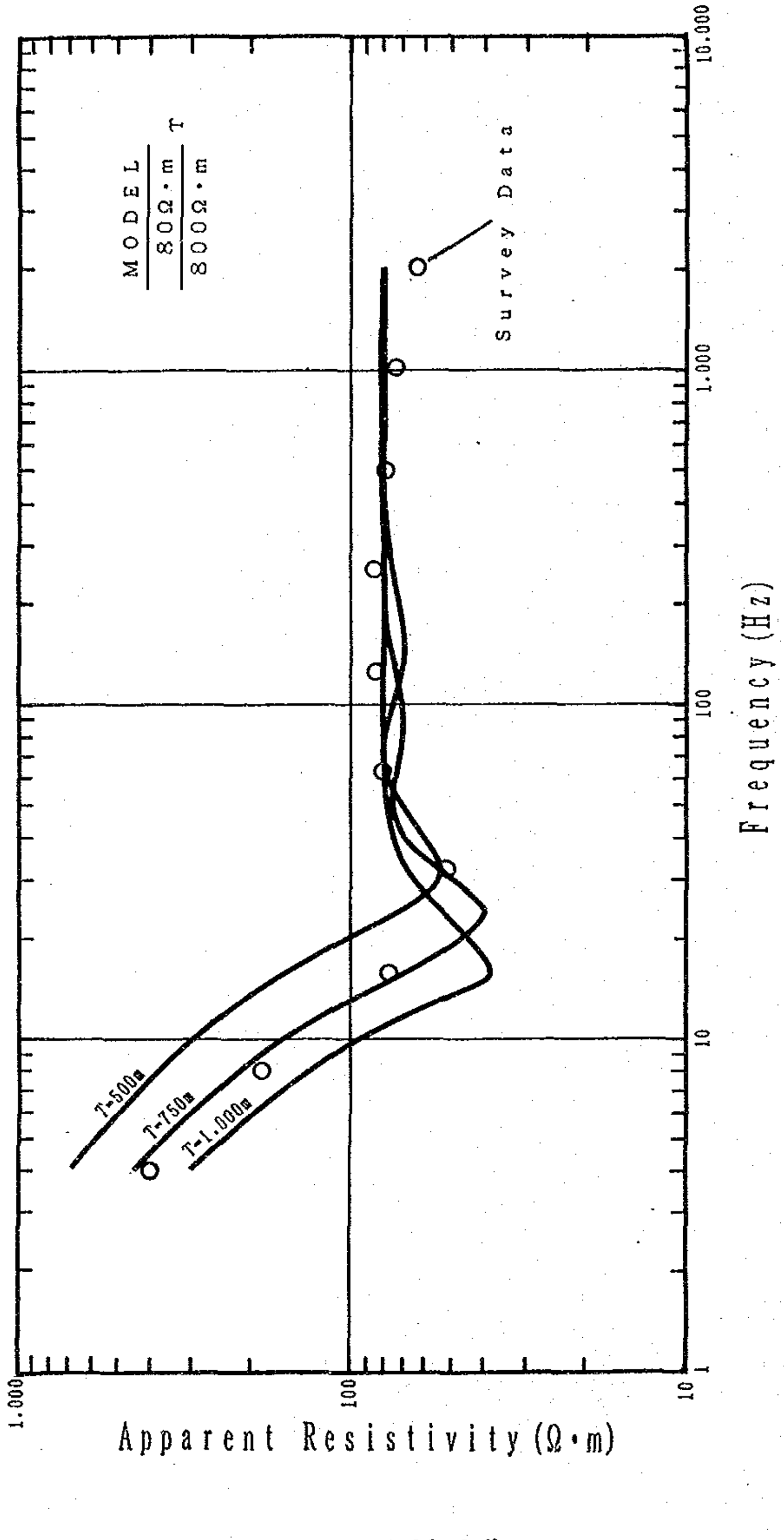

Fig.II－13 EM Modeling

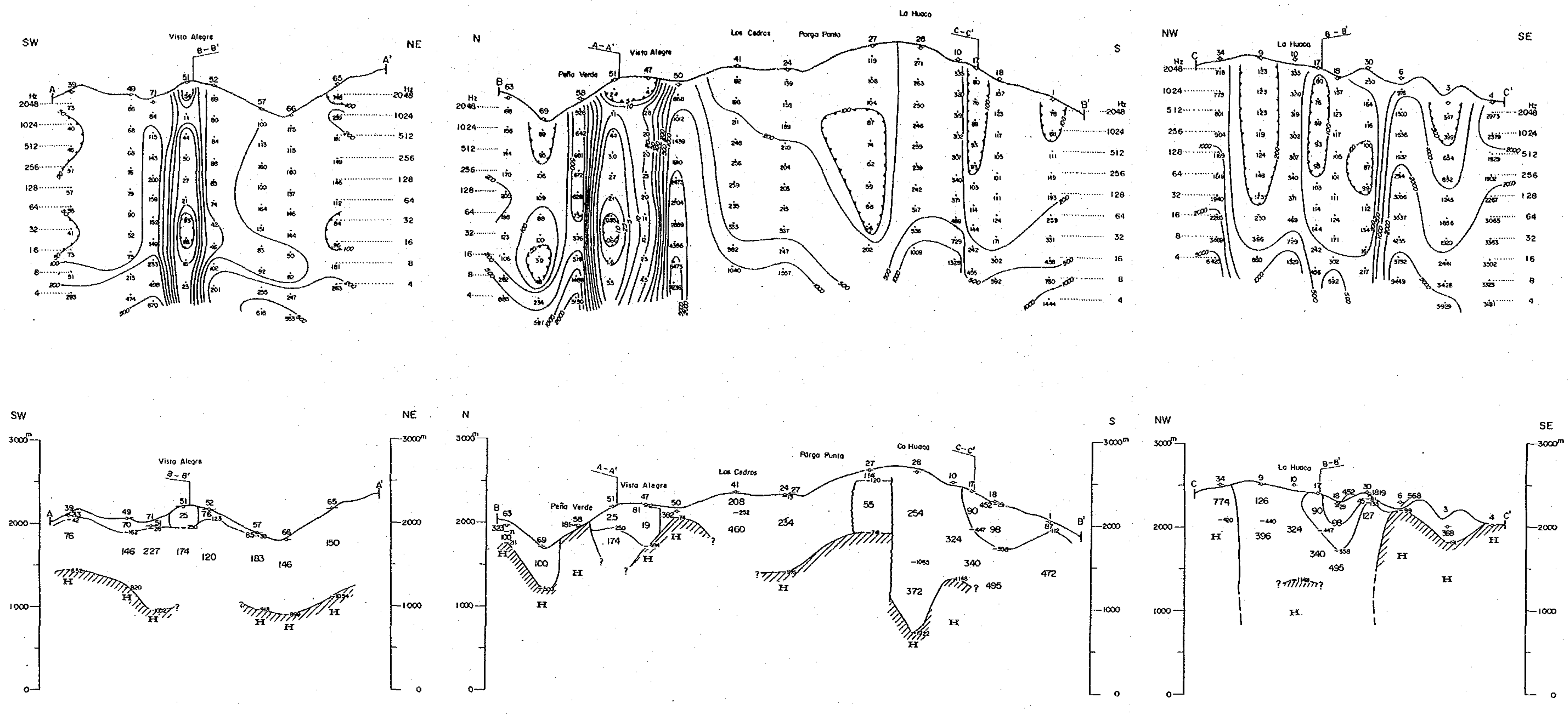

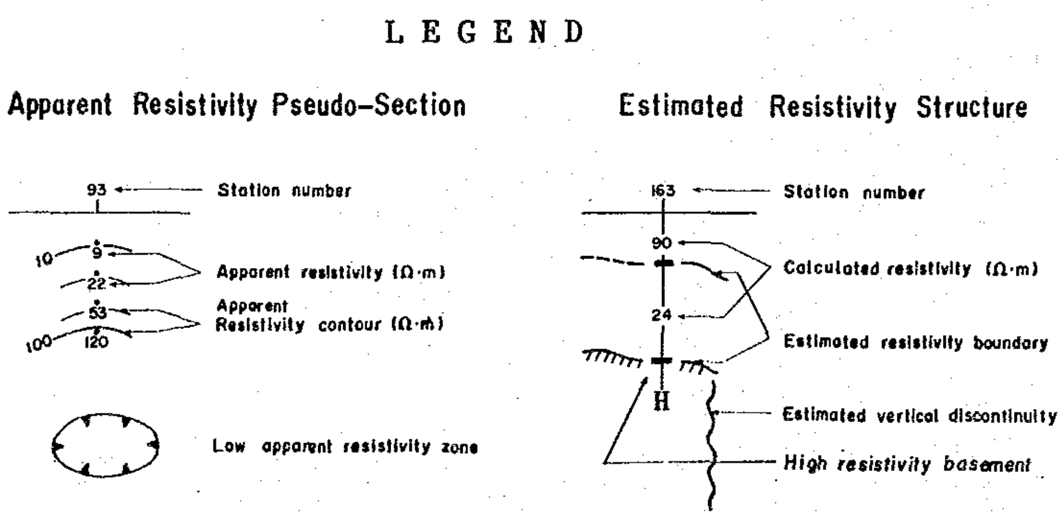

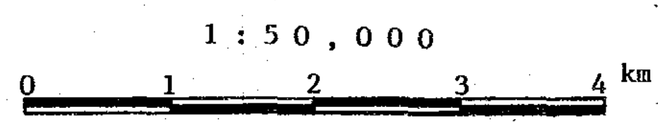

Fig.II–14 Apparent Resistivity Pseudo–Section with Estimated Resistivity Structure in The San Felipe Area

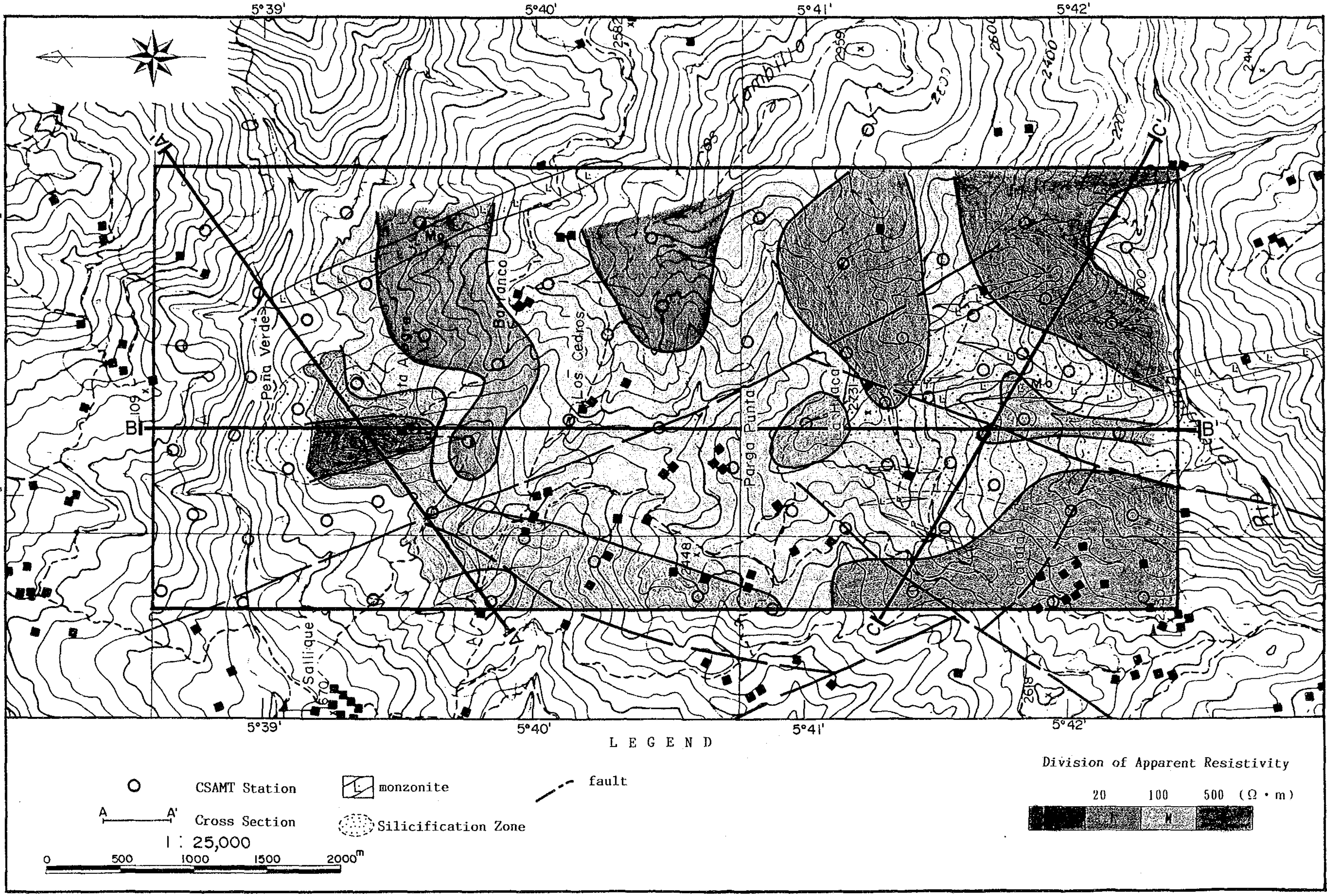

Fig.II−15 (1) Resistivity Structure Map of The San Felipe Area (+2,000m)

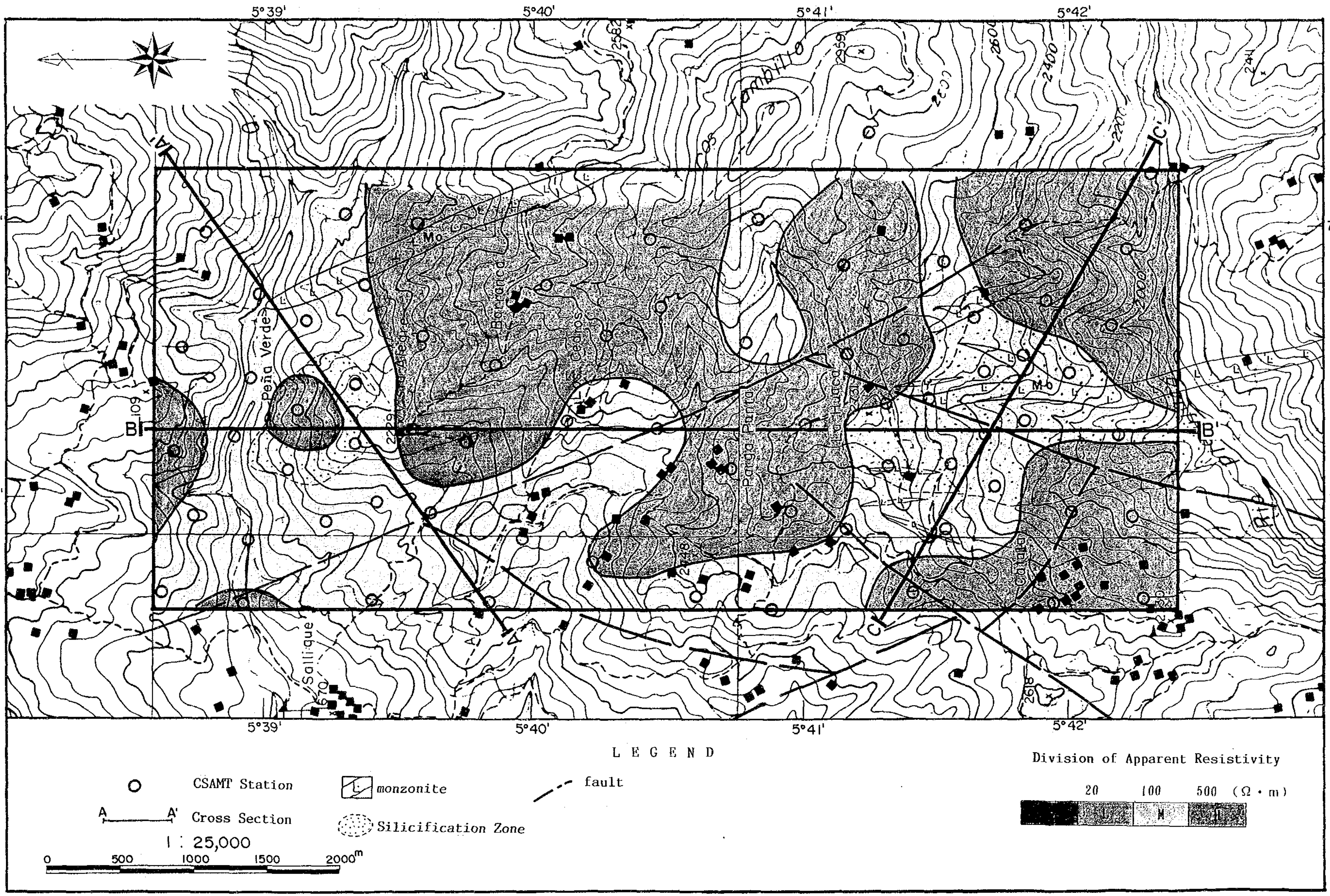

Fig.II−15 (2) Resistivity Structure Map of The San Felipe Area (+1,500m)

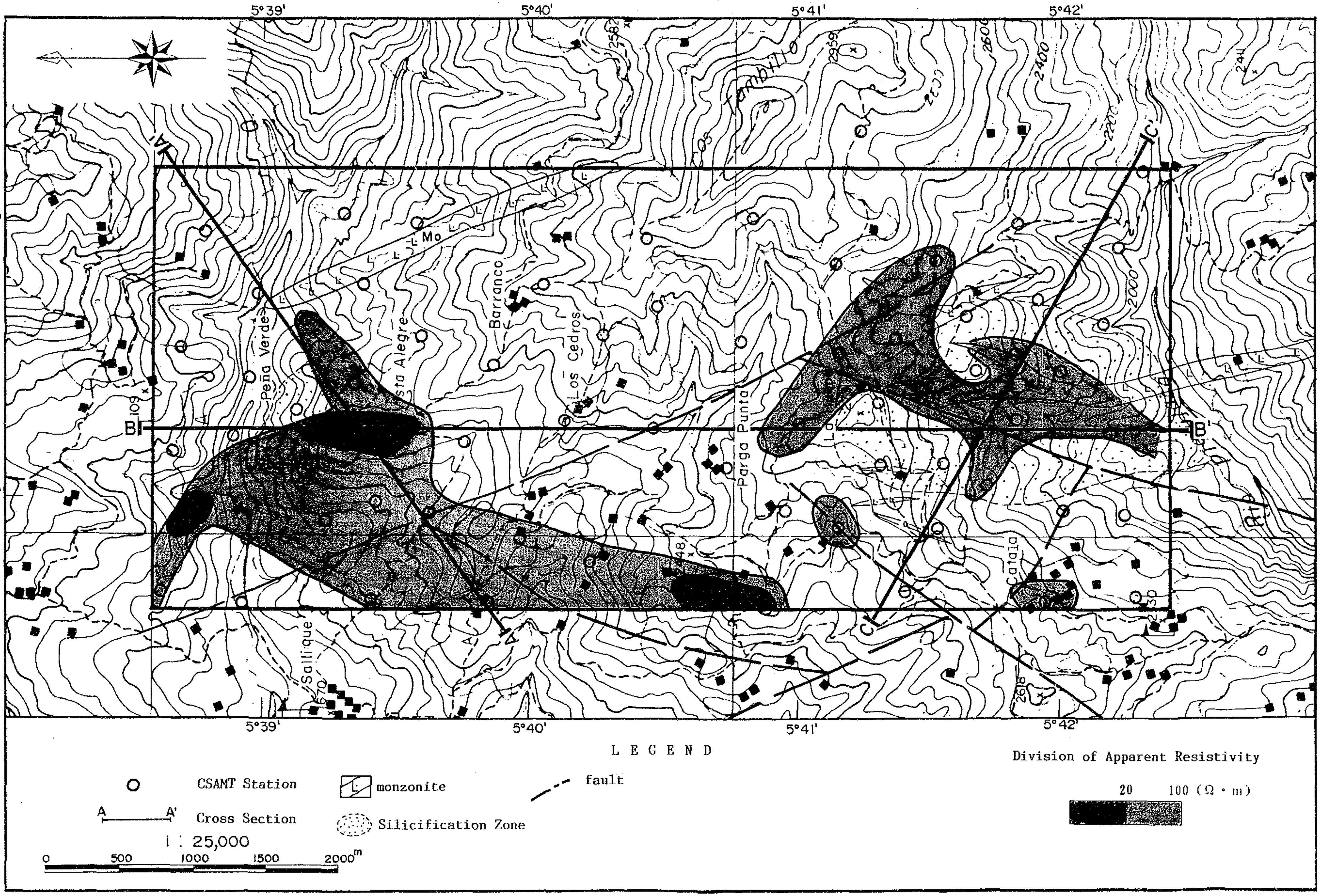

Fig.II—16 Low Resistivity Area Map of The San Felipe Area

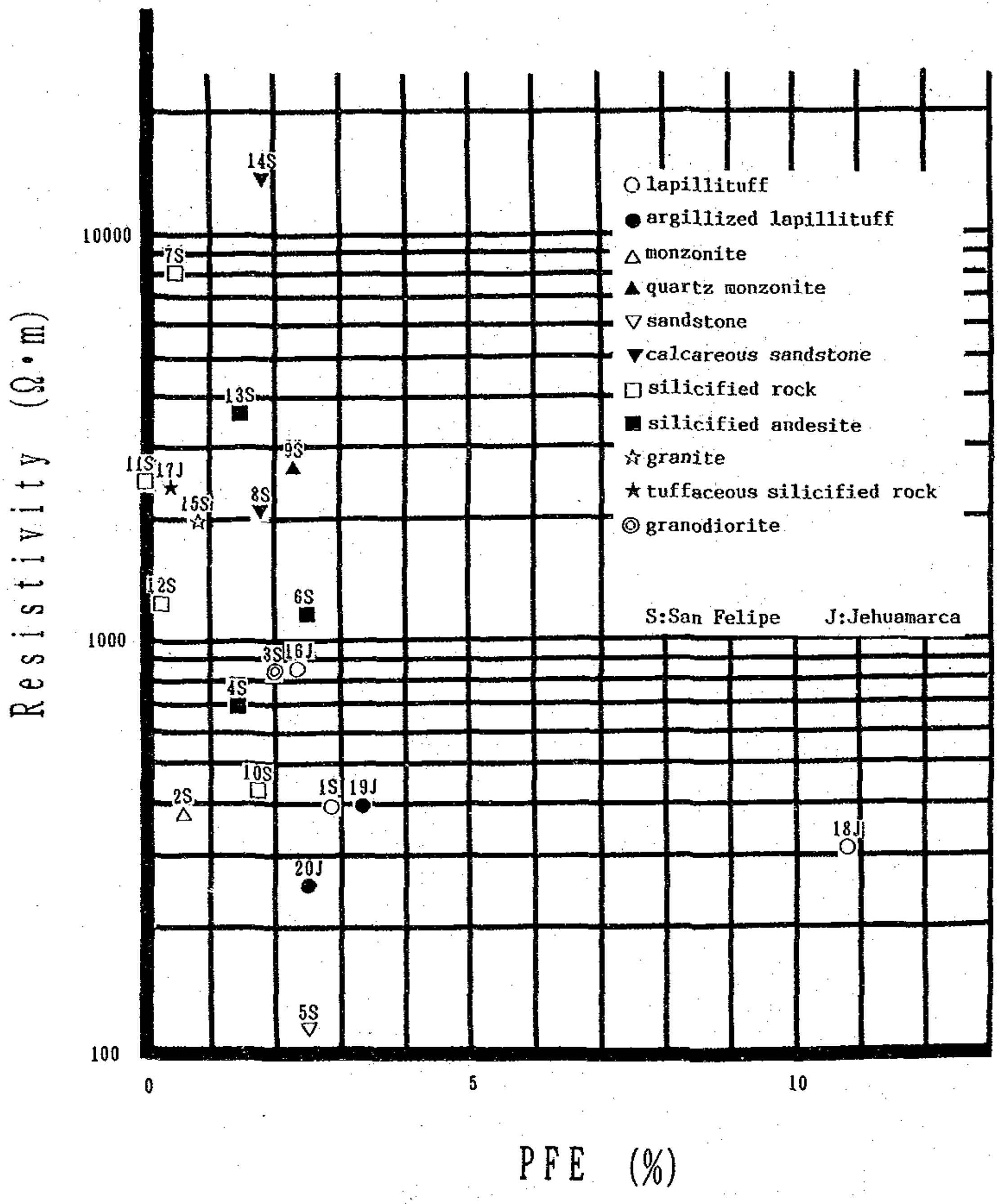

Fig.II−17 ρ−PFE Distribution of Rock Samples

2-3 Review (Consideration)

Geology of the San Felipe area consists of the Olmos Complex as basement, the Oyotun Volcanics, Goyllarisquizga Group, overlying Sedimentary rocks and intrusive rocks which intrude into them. The sedimentary rocks are mainly found in the western flange of this survey area, and is separated from the Oyotun Volcanics by fault systems of trendings NW-SE and NE-SW. The Oyotun Volcanics contain silicified and combined silicified and argillized zones having an approximate area of 2 km in width and 9 km in length in an almost north-south trending, containing the mineralized zones of Pena Verde, La Huaca and Vega previously detected. The geochemical survey verified the existence of zonal arrangements that includes copper, zinc and silver from the inside, centering on monzonite intruded zones in La Huaca, and that of silver anomaly corresponds to silicified zone with the distribution of the copper around. It is, therefore, likely that there are two types of mineralized alterations.

In the geophysical survey, basement rocks and non-altered volcanics are normally represented with medium to high resistivity. At La Huaca, low resistivity zones were verified with the center at monzonite which are distributed in the combined silicified and argillized zones. At Pena Verde, extremely low resistivity was detected, though on a small scale, to the south of the silicified zone previously verified at the surface. This could mean that the geophysical results also suggest the existence of two types of mineralized alterations.

In summary, it can be said that mineralization zones in La Huaca are attributable to the porphyry copper type mineralization. Based on this view, the distribution of molybdenum anomalous zones can be regarded as the external flange of such porphyry copper type mineralization, and therefore, the results of the boring conducted by BRGM had only been restricted to the findings at the western flange of the mineralized zones. The mineralizd zone in Pena Verde have the same characteristics with those of epithermal alteration as in the Jehuamarca area described in a later chapter.

CHAPTER 3 CHONTALI AREA

3-1 Purpose of the Survey and Procedure Used

The Chontali area concerns the zones where anomalies were extracted by geochemical survey using stream sediments as a part of the "Proyecto Integral Chinchipe". After this prospecting, no follow-up study was conducted. This year, the survey included a semi-detailed geological survey combined with geochemical survey for rock samples for the purpose of finding the source of the said anomalies.

The base camp was set up in the village of Chontali, located in the center of the survey area. No advance camp was set up because there is one road longitudinally crossing the area (Fig. I-1, I-2). With this road as the principal route for survey, riding trails were mainly used. In the same manner as in the case in San Felipe, a path-clearing team was formed for the virgin forests.

Five survey teams were organized between the Japanese engineers and their counterparts of Peru. Nightly discussions were held among team members regarding geological setting of each respective survey route and determing the next day's route.

Samples for geochemical analysis were taken at a relatively dense rate with emphasis on the primary objective of searching for the source of geochemical anomalous zone extracted by INGEMMET.

3-2 Geology

According to Reyes et al. (1987), this survey area consists of the Jurassic Oyotun Volcanics as basement, the Goyllarisquizga Group formed in the early Cretaceous Period over it and the diorites intruded into them (Fig. I-3).

The Oyotun Volcanics are mainly spread in the northern and eastern parts of the survey area. This area basically shows a simple geological structure as the general strike trending NW-SE and slightly dipping toward the southwest. The Goyllarisquizga Group is situated in the eastern part of the survey area, and diorites are found in its southwestern part.

3-3 Survey Results

1) Geological survey

The basement of this survey area is composed of crystalline schist and phyllite, which are covered by volcanic rocks unconformably. Over this sedimentary rocks are distributed also conformably, and intrusive rocks intrudeded into above mentioned geological units (Fig. II-18).

At the western flange of the area, crystalline schist and phyllite extend in the N-S to NW-SE trending. The schist consists of quartz-sericite schist and sericite-chlorite schiste. In the metamorphic rocks area, some arkose sandstones and/or quartzites boulder are occasionally found out, which suggest that these metamorphic rocks could be the source of pelitic rocks with intercalated sandy rocks. The crystalline schist containing phyllite trends N-S, with a slight undulating structures dipping gently to the west and east. This seems to indicate that there was no violent tectonic movement. Assessing from its rock facies, it is correlative with the Salas Group.

The volcanics are distributed at the central part of the area trending NW-SE, consist mainly of andesitic lavas, though containing tuff, tuff breccia and tuffaceous shale. The tuffaceous shale, which appears in the northwestern and southeastern parts of the area, corresponds to the lower part of the Volcanics. Although, tuff and tuff breccia occur in a small scale in all of the horizons, they cannot be used as key beds for the correlation of geologic formation site by site. In terms of geological structure, except some undulations, it presents a simple structure that basically trends NW-SE, with a gentle dipping to the northeast. The estimated thickness using an isopach mapping method shows about 1,600 meters(pl. 5). The age of these volcanic rocks cannot be readily determined because no fossils were present nor absolute age determination obtained. They, however, may be correlative with the Jurassic Oyotun Volcanics based on the assessment from their rock facies and the fact that they are intruded by igneous rocks belonging to the lower Cretaceous.

Sedimentary rocks are found out in the eastern part of the survey area. Though the relationship between these rocks and the underlying Oyotun Volcanics was not observed directly, it is assumed that these Volcanics almost conformably grade to sedimentary rocks at the upstream the Tabacal River in the eastern end of the area. Also, the general structure of these rocks are nearly concordant with the lower unit. Therefore, it is deemed that there is a conformable relationship between them. Their base consists of quartzite with well developed cross bedding, which grades into sandstone, alternation of shale and sandston, and limestone in ascending order. Further upper horizons are thickly covered with virgin forests, thus making it difficult to make some geological observations. Although no fossils were available from these sedimentary rocks, they may be correlative with the Goyllarisquizga Group and the calcareous formation (e.g., Inca Formation, Chulec Formation) belonging to the lower Cretaceous. Because they conformably cover the Oyotun Volcanics and are, on the other hand, intruded by monzonites.

Intrusive rocks in the area are found out from its western flange through to the southwestern part, and can roughly be classified into diorite-granodiorite, granite, monzonite, quartz porphyry-granite porplyries and andesite, in the same way as in the San Felipe area.

The diorite-granodiorite are found out in the southwestern part of the area across the Salas Group and Oyotun Volcanics. Through the reconnaissance prospection conducted along the Palma River, verification was made that these dioritic rocks were same intrusive body as in the Paramo zone of the San Felipe area, described in the preceding chapter. Under the microscope (Apx. 1), the texture of dioritic rock is a holocrystalline hypidiomorphic granular and rock facies vary from quartz-diorite consisting of plagioclase, biotite, hornblende, quartz and clinopyroxene (Sample No. K12309), to granodiorite consisting of plagioclase, quartz, pottasium feldspar and biotite (Sample No. H12405 B). The absolute age of Sample No. K12309 is estimated at 119±6 million years using the K/Ar method, thus giving the solidification age is in Aptian (upper of the Early Cretaceous).

Granite is found out at two localities, at the western and southwestern flanges of the survey area, intruding through the diorite-granodiorite body. Megascopically it is peculiarly coarse grained. Microscopically, this is the so-called quartz monzonite consisting of potassium feldspar, plagioclase, quartz, biotite and hornblende (Sample No. H12418). The absolute age of Sample No. H12418 is estimate at 106±5 million years (Albian) using the K/Ar method, which coincides with the results of the observation in the field, that identified it younger than the dioritic rocks. Monzonite appears as dykes throughout the area in scales of about several meters to 200 m in width and 10 m to 4 km in length. Under the microscope, its texture is holocrystalline porphyritic and mineral component consists of plagioclase, quartz and altered minerals as calcite and sericite (Sample No. K12501), and shows its facies as the so-called quartz monzonite porphyry. Quartz-granite porphyries appear as small scaled dykes in the distribution areas of diorite-granodiorite, granite and in their periphery. These porphyries show, under the microscope (Apx. 1), a holocrystalline equigranular or porphyritic to granophyre texture, and vary from granite porphyry (H12404) consisting of plagioclase, quartz and potassium feldpar as phenocrysts, and plagioiclase, quartz and altered minerals as chlorite, sericite and clinozocite as matrix. Andesite appears as small-scale dykes in the whole survey area.

Fault-fissure system in this area could not be identified during the field survey. Based on the airphotograph analysis, used as an auxiliary means, significant two lineaments with trending NNE-SSW to NE-SW were extracted at central and

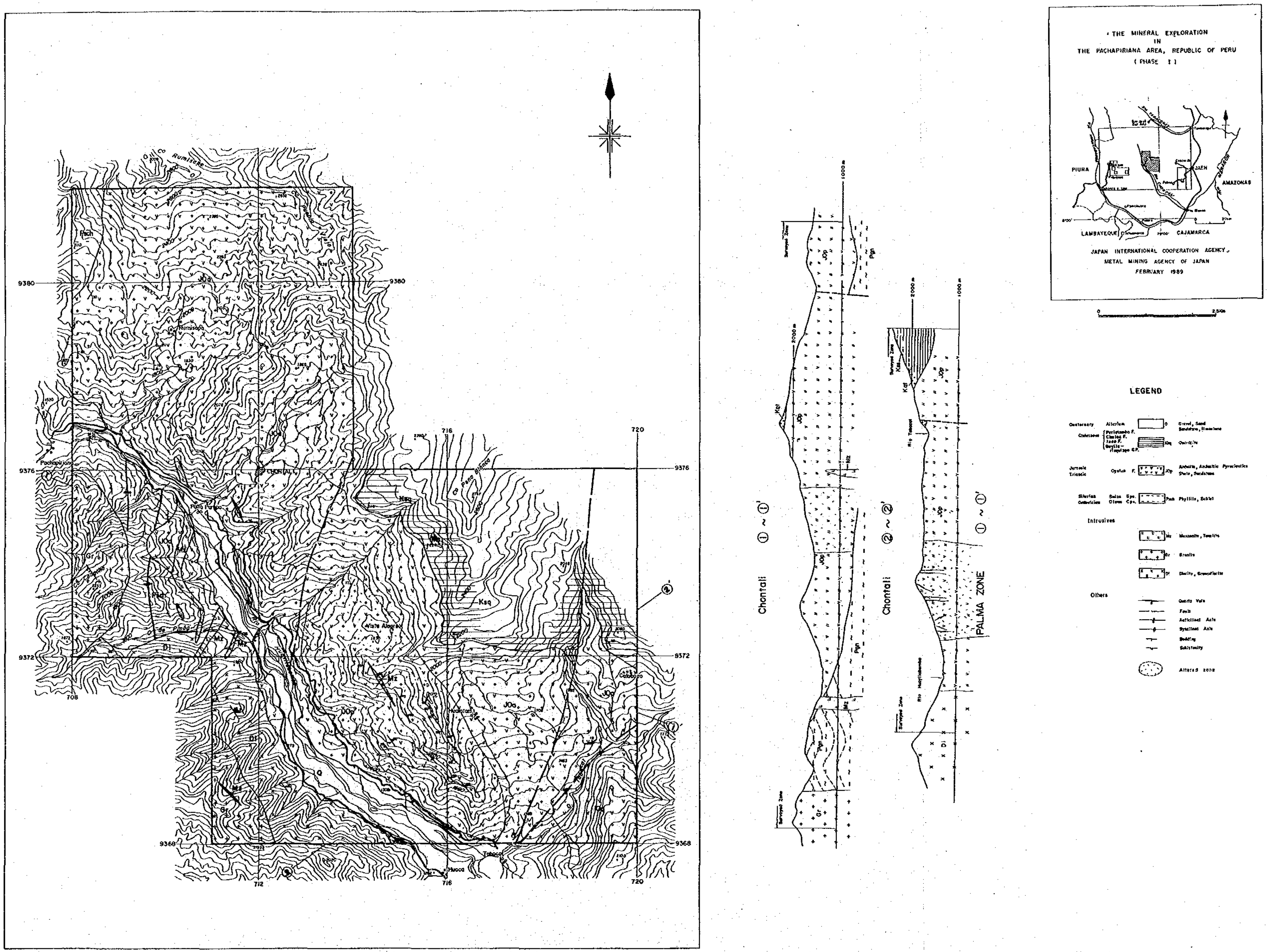

Fig.II－18　Geological Map and Profiles of The Chontali Area

southeastern part of the area. Of these two, the one at the southeastern part is supposed to be a relatively large-scaled fault as it apparently dislocated the Goyllarisquizga Group quartzite about 500 meters vertically(pl. 5), and small discordant out crop of schist, which would be removed by a tectonic movement, are observed near the lineament.

Alteration in this area occurs in the Oyotun Volcanics which is located between the lineaments mentioned above. This alteration is considered to be attributable to the hydrothermal effects centered at the NW-SE trending fracture and extending in the same direction and its scale is 2 km in width and 6 km in length. The NW-SE fracture is generally accompanied with minor scaled silicified zone and occasionally forming quartz veins, which measure 0.1 to 1 meter in width and several ten to hundred meters in length on the average, sometimes reaching the maximum width of 4 meters and 300 meters in length. The occurrence frequency of these veins flactuate depending on a locality, but they are present over the entire alteration zone. The small-scale silicification zones (with an average width of 1 meter or less) are surrounded by combined silicified and argillized and/or argillized zones, and gather them to be formed the above-mentioned large-scale alteration distribution zone. It was verified that these alteration zones were also found in the extension of the southeast of the survey area. As a result of an X-ray diffractive analysis (Apx. 5), quartz, sericite, smectite, halloysite, mixed layer of sericite and semctite, and kaolinite, which are the characteristic hydrothermal alteration minerals, were detected. Also goethite and/or hematite were characteristically associated, suggesting the existance of sulphide minerals.

2) Geochemical survey

Compared with other semidetaited suevey areas based on the average values (Table II-2), a high concentration of zinc (253.18 ppm) is observed in this Chontali area. Analyzing the distribution of anomalous zones per each element, it is noted that those of gold, silver, lead and molybdenum are widely sporadic and moreover, very small in scale. Those of zinc and copper appear in a relatively wide range, but low in concentrations. It is also characteristic in the area that the distribtuion of anamalous zones for each element rarely overlap.

In a general view (Fig. II-19(1),(2)), geochemically anomalous zones of gold, silver and molybdenum are concentrated in the south of the area, those of lead south of the center, and those of zinc and copper almost throughout the area.

In terms of correlation with the geological units, the anomalous values of gold and silver are distributed in the alteration zones and their neighboring areas

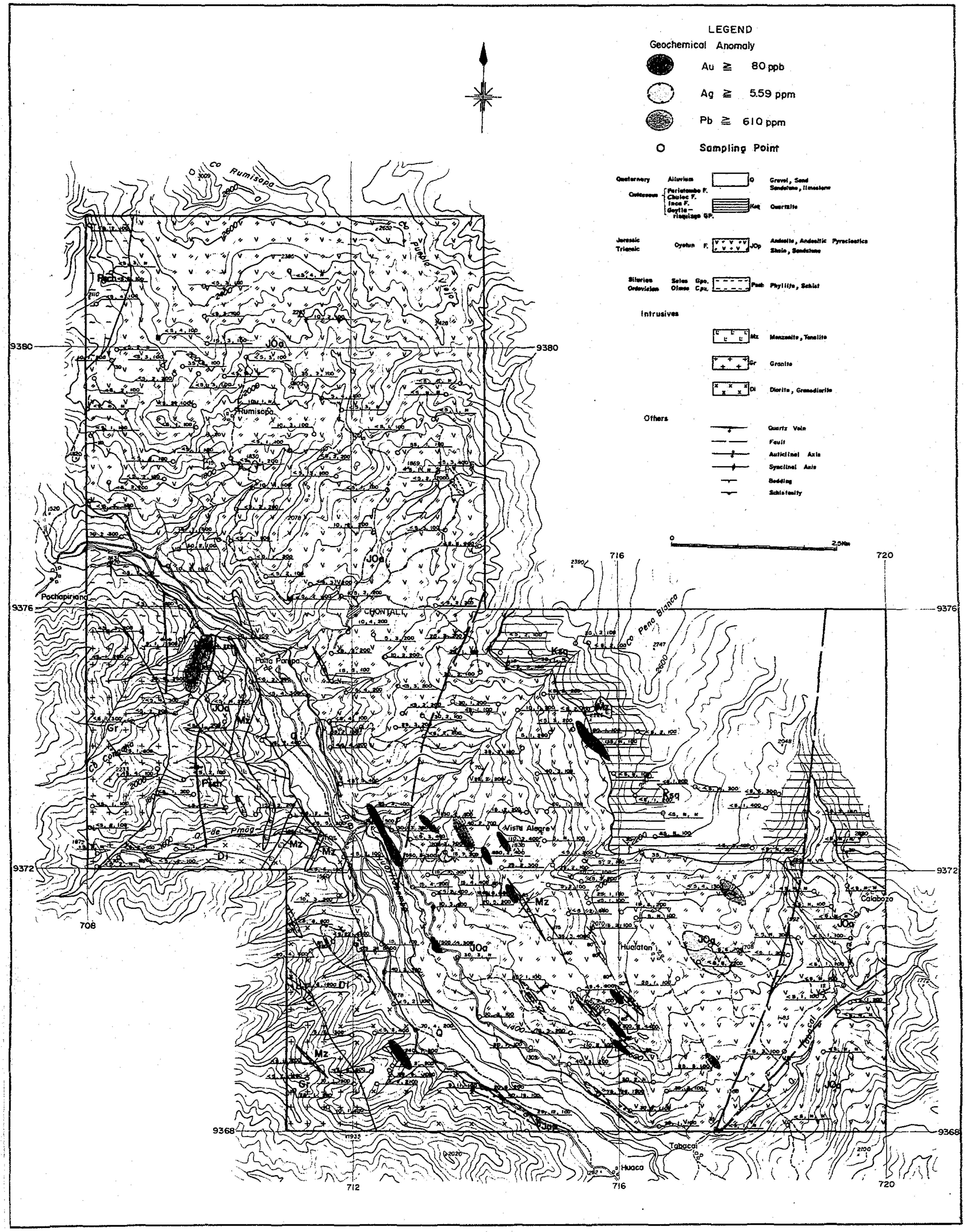

Fig.II−19 (1) Geochemical Map of The Chontali Area (Au. Ag and Pb)

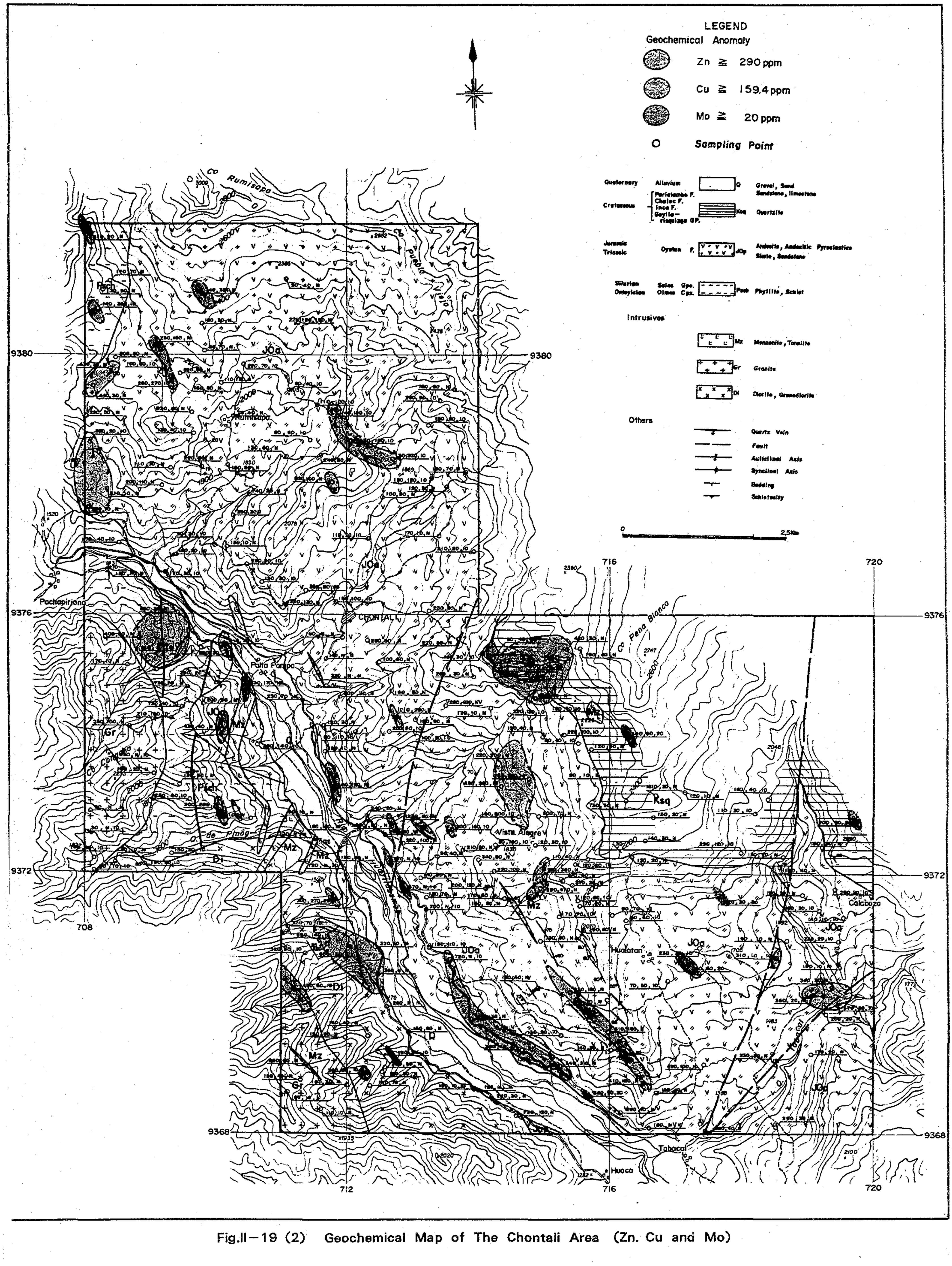

Fig.II−19 (2) Geochemical Map of The Chontali Area (Zn. Cu and Mo)

where the distribution of diorite-granodiorite is predominant. In case of the silver anomaly, quartz porphyry, quartz vein and/or fractured zone that can serve as their passage are always identified. The anomalous zones of lead are similar to those for gold and silver and arranged in such a manner that the former surround the latter. These anomalous zones trend in concordance with schistosity of the basement. Anomalous zones of molybdenum also surrounded those of silver, without any anomaly in the basement, also found out in the quartzite, sandstone and limestone of the Goyllarisquizga Group. With respect to zinc, its anomaly is distributed widely thoughout whole of the geological units, and it is noticeable that relatively higher values are found out in the basement. Distribution of anomalous zones of copper also covers the entire area except in the Goyllarisquizga Group, where no anomaly was observed; also scare distribution in the basement, but predominantly distributed in the Oyotun Volcanics and intrusive rocks.

3-4 Results of Chemical Analysis of Ore

Laboratory tests were conducted on seventeen rock samples from the quartz veins produced in the alteration zones in the survey area, which showed the presence of limonite and/or goethite deemed to have originated sulphides, and two samples showing dissemination of pyrite from the altered rocks. The assay results are shown in Apx. 8.

Grades of quartz vein samples by arithmetic means were 1.37 g/ton Au, 7.4 g/ton Ag, 358.8 ppm Pb, 201.8 ppm Zn, 65.3 ppm Cu and 4.1 ppm Mo; and the mean grades of altered rock samples, 0.20 g/ton Au, 12.58 g/ton Ag, nil Pb, 210 ppm Zn, 60 ppm Cu and 5 ppm Mo; thus providing evidence that auri-argentiferous mineralization is predominant in the area, particularly with gold as its maximum grade was recorded at 10.3 g/ton. Therefore, it is very probable that there are ore deposits of gold.

3-5 Review

The Chontali area consists of the Salas Group schist as basement, the Oyotun Volcanics, Goyllarisquizga Group, Sedimentary rocks and intrusive rocks which interude into the formers. Structurally, there is little disturbance, with only two lineaments trending NE-SW extracted by airphotograph analysis. In the zone between these two lineaments, combined alterations (silicification and argillization) were predominant, in which there were abundant quartz veins. Macroscopically, these alteration zones trend NE-SW in which the quartz veins appear in the same direction; microscopically, they occur in close contact with the quartz veins. These facts lead the conclusion that silicification and/or combined silicification and argillization originate from the same source of quartz vein formation.

Auri-argentiferous mineralizations are inherent to the quartz veins, and in consideration that some samples and ore deposit grade at surface exposure, it is concluded that this area has high possibility of an existance of epithermal vein type gold and silver deposits.